Progress In Electromagnetics Research, PIER 86, 135–154, 2008

A TWO-SLOT ARRAY ANTENNA ON A CONCENTRIC SECTORAL CYLINDRICAL CAVITY EXCITED BY A COUPLING SLOT

P. Wounchoum

Department of Telecommunication Engineering
Faculty of Engineering
King Mongkut's Institute of Technology Ladkrabang
Bangkok 10520, Thailand

D. Worasawate

Department of Electrical Engineering
Faculty of Engineering
Kasetsart University
Bangkok 10900, Thailand

C. Phongcharoenpanich and M. Krairiksh

Department of Telecommunication Engineering
Faculty of Engineering
King Mongkut's Institute of Technology Ladkrabang
Bangkok 10520, Thailand

Abstract—A two-slot array antenna on a concentric sectoral cylindrical cavity excited by a coupling slot is investigated. The electromagnetic fields and Q factors for the first few modes of a concentric sectoral cylindrical cavity are presented. It shows that the appropriate mode for a slot array antenna on a concentric sectoral cylindrical cavity is the TM_{110} mode. The correlations between each mode distribution and the magnetic field distributions inside the cavity are presented. The antenna design and the parametric study of a two-slot array antenna on a concentric sectoral cylindrical cavity for a single sector are illustrated. Simulated results are validated by measurements. The results provide useful information for the design of a switched-beam slot array antenna on the concentric sectoral cylindrical cavities.

1. INTRODUCTION

Slot array antennas have been widely used for many applications due to its conformal nature, compact structure, high power handing, and high efficiency. Many researches on slot antennas have been extensively studied on different structures such as rectangular waveguides [1–7], spheroids [8], infinitely long cylinders [9–11], circular cylindrical cavities [12] and coaxial cables [13–17]. Slot antennas on sectoral cylindrical waveguides have been studied in [18–22]. An impedance characteristic of a sectoral cylindrical cavity-backed slot antenna excited by a probe was presented by [23, 24]. To the best of our knowledge, a concentric sectoral cylindrical cavity-backed slot array antenna excited by a coupling slot has not been analyzed.

This paper focuses on a two-slot array antenna on a concentric sectoral cylindrical cavity excited by a coupling slot. All slots are circumferentially oriented. The antenna is intended for using in a wireless sensor network. A switched-beam antenna, compositing of several antennas covering different sensing areas, is desirable for a master node. The operating frequency of 5.8 GHz ISM band is used for the sensor-size minimization. The goal of this paper is to study the magnetic field distributions inside the slotted cavity and the effects on the antenna characteristics. The magnetic fields for the first few modes inside the cavity with the sectoral angle of 60 degrees are presented. The dimensions of the cross section of the cavity are obtained by considering the solutions for a coaxial cylindrical cavity given in [25, 26] and a circular sectoral waveguide given by [20]. The relations between the outer radius (in terms of wavelength) and the ratio of the inner to outer radii are illustrated. The results show the effects of these parameters on the TM_{110} mode which is easily excited by a coupling slot and provide a uniformly distributed magnetic field on the outer metal wall. Q factors are obtained from the losses of metal wall by using the surface impedance method [25–27]. The Q factor is used to set the optimum dimensions of the cavity. The relations between the ratio of the inner to outer radii and the Q factor are illustrated for TM_{11q} modes. The correlations between each mode distribution and the magnetic field distributions inside the cavity are presented. Computer Simulation Technology (CST) was used as a simulation tool to obtain the antenna characteristics. The radiation pattern, magnetic field distribution and magnitude of S_{11} are investigated in the terms of the length of the cavity. The location of the coupling slot is considered to find the appropriate antenna characteristics. The prototyped antenna was fabricated and measured to verify the simulated results. The results provide useful information for the design of a switched-beam slot array antenna on the concentric sectoral cylindrical cavities.

2. CONCENTRIC SECTORAL CYLINDRICAL CAVITY

2.1. Electromagnetic Solutions for a Concentric Sectoral Cylindrical Cavity

The geometry of a concentric sectoral cylindrical cavity is shown in Fig. 1. The inner and outer radii of the cavity are denoted by r_a and r_b, respectively. The cavity is enclosed by conducting surfaces at the angles of $\phi = \phi_1$ and $\phi = -\phi_1$. The height of the cavity is denoted by l_R where the bottom and top of the cavity are at $z = 0$ and $z = l_R$, respectively. The cavity is filled with a dielectric medium with the permittivity of ε and permeability of μ. The electric field, **E**, and magnetic field, **H**, in the cavity can be derived from the magnetic vector potential, **A**, and the electric vector potential, **F** as [27]

$$\mathbf{E}(\mathbf{r}) = \frac{1}{j\omega\mu\varepsilon}\nabla \times \nabla \times \mathbf{A}(\mathbf{r}) - \frac{1}{\varepsilon}\nabla \times \mathbf{F}(\mathbf{r}) \quad (1)$$

$$\mathbf{H}(\mathbf{r}) = \frac{1}{j\omega\mu\varepsilon}\nabla \times \nabla \times \mathbf{F}(\mathbf{r}) + \frac{1}{\mu}\nabla \times \mathbf{A}(\mathbf{r}) \quad (2)$$

These electromagnetic fields can be decomposed into two separated modes: TE and TM modes. For TE modes, **A** vanishes and only the z-component of **F** exists. For TM modes, **F** vanishes and only the z-component of **A** exists. The expressions for the fields of a concentric sectoral cylindrical cavity are obtained by modifying the solutions of a coaxial cylindrical cavity and a circular sectoral waveguide.

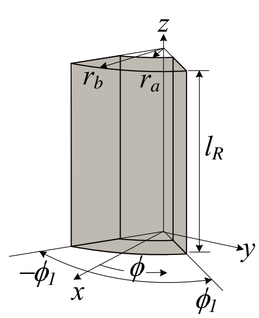

Figure 1. Geometry of a concentric sectoral cylindrical cavity.

The expressions for the fields of TE modes are written as

$$\mathbf{F} = A_{pn} B_{\mathrm{TE}}(\rho) \cos(m\phi) \sin(\beta z) \mathbf{a}_z \tag{3}$$

$$E_\rho = A_{pn} \frac{m B_{\mathrm{TE}}(\rho)}{\varepsilon \rho} \sin(m(\phi - \phi_1)) \sin(\beta z) \tag{4}$$

$$E_\phi = A_{pn} \frac{B'_{\mathrm{TE}}(\rho)}{\varepsilon} \cos(m(\phi - \phi_1)) \sin(\beta z) \tag{5}$$

$$E_z = 0 \tag{6}$$

$$H_\rho = A_{pn} \frac{\beta B'_{\mathrm{TE}}(\rho)}{j\omega\mu\varepsilon} \cos(m(\phi - \phi_1)) \cos(\beta z) \tag{7}$$

$$H_\phi = -A_{pn} \frac{m\beta B_{\mathrm{TE}}(\rho)}{j\omega\mu\varepsilon\rho} \sin(m(\phi - \phi_1)) \cos(\beta z) \tag{8}$$

$$H_z = A_{pn} \frac{k_c^2 B_{\mathrm{TE}}(\rho)}{j\omega\mu\varepsilon} \cos(m(\phi - \phi_1)) \sin(\beta z) \tag{9}$$

where subscripts ρ, ϕ, and z denote the radial, circumferential, and axial components of the fields and the A_{pn} values are the amplitudes of the modes associated with subscripts $p = 0, 1, 2, \ldots,$ $n = 1, 2, 3, \ldots$ and $m = p\pi/2\phi_1$. The function $B_{\mathrm{TE}}(\rho)$ and its derivative $B'_{\mathrm{TE}}(\rho)$ are defined as

$$B_{\mathrm{TE}}(\rho) = N_m\left(x'_{pn}\frac{\rho}{r_a}\right) - \frac{N'_m(x'_{pn})}{J'_m(x'_{pn})} J_m\left(x'_{pn}\frac{\rho}{r_a}\right) \tag{10}$$

$$B'_{\mathrm{TE}}(\rho) = \frac{x'_{pn}}{r_a}\left[N'_m\left(x'_{pn}\frac{\rho}{r_a}\right) - \frac{N'_m(x'_{pn})}{J'_m(x'_{pn})} J'_m\left(x'_{pn}\frac{\rho}{r_a}\right)\right] \tag{11}$$

where x'_{pn} is a root of

$$J'_m(x'_{pn}) N'_m(x'_{pn} r_b/r_a) - N'_m(x'_{pn}) J'_m(x'_{pn} r_b/r_a) = 0 \tag{12}$$

and J_m, J'_m and N_m, N'_m are Bessel functions and their derivatives of order m of the first and second kinds, respectively.

The expressions for the fields of TM modes are written as

$$\mathbf{A} = B_{pn} B_{\mathrm{TM}}(\rho) \sin(m(\phi - \phi_1)) \cos(\beta z) \mathbf{a}_z \tag{13}$$

$$E_\rho = -B_{pn} \frac{\beta B'_{\mathrm{TM}}(\rho)}{j\omega\mu\varepsilon} \sin(m(\phi - \phi_1)) \sin(\beta z) \tag{14}$$

$$E_\phi = -B_{pn} \frac{m\beta B_{\mathrm{TM}}(\rho)}{j\omega\mu\varepsilon\rho} \cos(m(\phi - \phi_1)) \sin(\beta z) \tag{15}$$

$$E_z = B_{pn} \frac{k_c^2 B_{\mathrm{TM}}(\rho)}{j\omega\mu\varepsilon} \sin(m(\phi - \phi_1)) \cos(\beta z) \tag{16}$$

$$H_\rho = B_{pn} \frac{m B_{\mathrm{TM}}(\rho)}{\mu\rho} \cos(m(\phi - \phi_1)) \cos(\beta z) \tag{17}$$

$$H_\phi = -B_{pn} \frac{B'_{\mathrm{TM}}(\rho)}{\mu} \sin(m(\phi - \phi_1)) \cos(\beta z) \tag{18}$$

$$H_z = 0 \tag{19}$$

where the B_{pn} values are the amplitudes of the modes associated with subscripts $p = 1, 2, 3, \ldots,$ $n = 1, 2, 3, \ldots$ and $m = p\pi/2\phi_1$. The function $B_{\mathrm{TM}}(\rho)$ and its derivative $B'_{\mathrm{TM}}(\rho)$ are defined as

$$B_{\mathrm{TM}}(\rho) = N_m\left(x_{pn}\frac{\rho}{r_a}\right) - \frac{N_m(x_{pn})}{J_m(x_{pn})} J_m\left(x_{pn}\frac{\rho}{r_a}\right) \tag{20}$$

$$B'_{\mathrm{TM}}(\rho) = \frac{x_{pn}}{r_a}\left[N'_m\left(x_{pn}\frac{\rho}{r_a}\right) - \frac{N_m(x_{pn})}{J_m(x_{pn})} J'_m\left(x_{pn}\frac{\rho}{r_a}\right)\right] \tag{21}$$

where x_{pn} is a root of

$$J_m(x_{pn}) N_m(x_{pn} r_b/r_a) - N_m(x_{pn}) J_m(x_{pn} r_b/r_a) = 0. \tag{22}$$

The relation between k, k_c, and β is given by $k^2 = k_c^2 + \beta^2$ where $k = \omega\sqrt{\mu\varepsilon} = 2\pi/\lambda$ is a wavenumber in the dielectric-filled medium and

$$\beta = \frac{q\pi}{l_R}, \quad \begin{cases} q = 1, 2, 3 \ldots. & \text{for } \mathrm{TE}^z_{pnq} \text{ modes} \\ q = 0, 1, 2 \ldots. & \text{for } \mathrm{TM}^z_{pnq} \text{ modes} \end{cases} \tag{23}$$

where $k_c = \frac{x'_{pn}}{r_a}$ for TE^z_{pn} modes and $k_c = \frac{x_{pn}}{r_a}$ for TM^z_{pn} modes.

Equations (12) and (22) show that the roots x'_{pn} and x_{pn} are functions of the ratio of the inner to outer radii, r_a/r_b. To obtain k_c for each mode, the ratio r_a/r_b and one of two radii must be given.

The quality factor or the Q factor is given by

$$Q = \frac{2\pi f_r W}{P_d} \tag{24}$$

where W is the energy stored in the cavity, P_d is the losses of the metal walls, and f_r is the resonant frequency. Their expressions are given as

$$W = \frac{\varepsilon}{2} \int_{Vol} |\mathbf{E}|^2 \, dv \tag{25}$$

$$P_d = \frac{R_s}{2} \oint_S |\mathbf{a}_n \times \mathbf{H}|^2 \, ds \tag{26}$$

$$f_r = \frac{1}{2\pi\sqrt{\mu\varepsilon}} \sqrt{(k_c)^2 + \left(\frac{q\pi}{l_R}\right)^2} \tag{27}$$

where $\int_{Vol}$ denotes the volume integration over the cavity, $\oint_S$ denotes the surface integration over the surface of the cavity, $\mathbf{a}_n$ is a unit vector pointing outward from the surface of the cavity, and the surface impedance at the resonant frequency is given by $R_s = \sqrt{\pi f_r \mu / \sigma}$. It can be derived from Eqs. (24)–(26) that the Q factor is inversely proportional to $\sqrt{f_r}$ when the electrical dimensions are fixed. In this paper, copper with the conductivity of $\sigma = 5.84 \times 10^7$ S/m is used as the metal wall and the cavity is filled with free space.

2.2. Magnetic Field Distribution inside a Concentric Sectoral Cylindrical Cavity

The magnetic field distributions inside a concentric sectoral cylindrical cavity for individual mode are obtained from Eqs. (7)–(9) and Eqs. (17)–(19) for the TE and TM modes, respectively. The sectoral angle of 60 degrees (ϕ_1 is equal to 30 degrees) is chosen such each antenna covers one of the six regions which the omnidirectional pattern is equally divided. Fig. 2 shows the geometry of xy-plane, xz-plane, and yz-plane that will be used to refer the magnetic field distribution. The magnetic field distributions inside the cavity for the first few modes are plotted, as shown in Figs. 3–5. It is observed that the TM_{110} mode (dominant mode of TM mode) provides a uniform distribution of magnetic field on the curved metal wall and the magnetic field is aligned in ϕ direction. The appropriate mode for a circumferential slot array antenna is the TM_{110} mode. The TE_{11q} modes can be excited

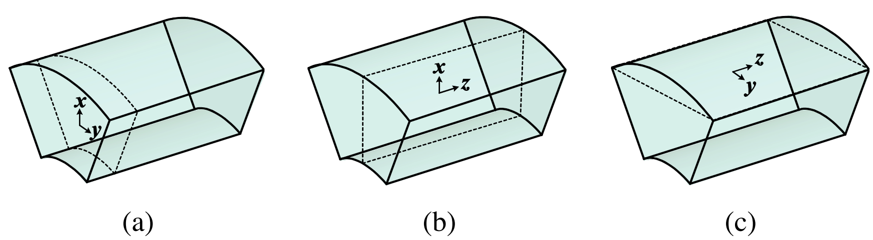

Figure 2. Principal planes for consideration of magnetic field distribution: (a) xy-plane, (b) xz-plane, (c) yz-plane.

when the coupling slot is located at the strong magnetic field position, but do not provide a uniform distribution of magnetic field on the curved metal wall. The TE_{01q} modes cannot be excited by the coupling slot because the magnetic field is aligned in the z direction. Therefore, the distribution of magnetic field of the TM_{110} mode can be easily excited by a coupling slot.

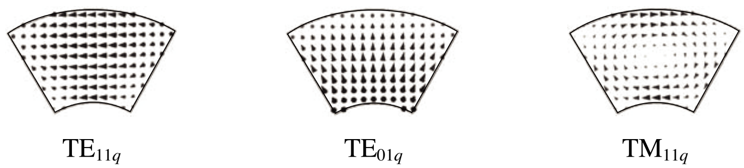

Figure 3. Magnetic field inside the cavity in the xy-plane.

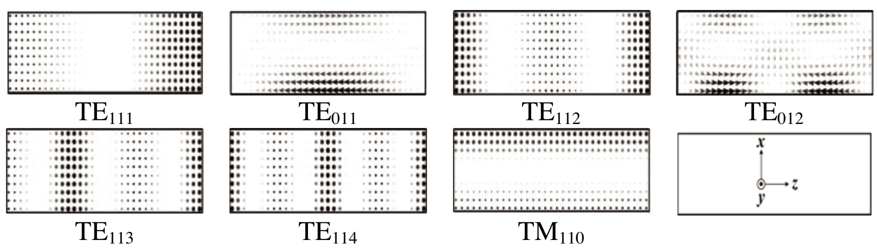

Figure 4. Magnetic field inside the cavity in the xz-plane.

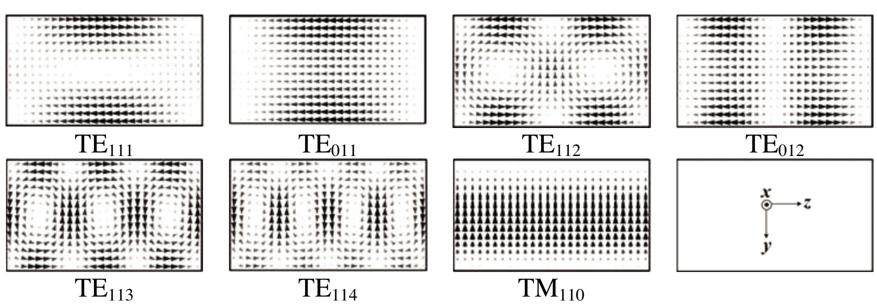

Figure 5. Magnetic field inside the cavity in the yz-plane.

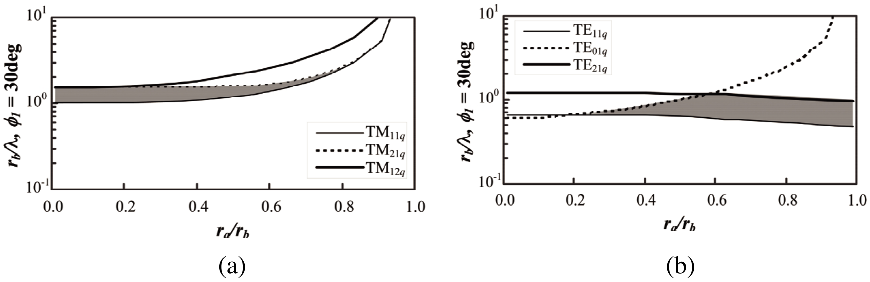

Figure 6. Mode loci for the TE and TM modes: (a) TM, (b) TE.

2.3. Effects of Dimensions of the Cross Section on Dominant Modes and Q Factors

This section discusses the effects of the dimensions of the cross section of the cavity on dominant modes using mode loci. The mode locus of each mode is the relation between r_b/λ and r_a/r_b for which k is equal to k_c for the specific mode. These relations are obtained from Eqs. (12) and (22). The mode loci for the first few modes are shown in Figs. 6(a) and 6(b) for the TE modes and TM modes. Assuming that only either the TE or the TM modes are excited, the lowest locus indicates the dominant mode. Fig. 6(a) shows the mode loci for the TM modes with $\phi_1 = 30°$. The TM_{11q} mode is a dominant mode for all r_a/r_b. However, the width of the valid region for the TM_{11q} mode decreases as r_a/r_b increases. The parameters for which the TM_{11q} mode exists as a single mode are obtained in the shaded region called the valid region. Fig. 6(b) shows the mode loci for the TE modes with $\phi_1 = 30°$. The results show that the dominant mode TM_{11q} is higher mode of the TE_{11q} mode and TE_{01q} mode. The resonant frequency of TM_{110} is the smallest value of r_b/λ in the valid region.

The Q factor is used to choose the optimum dimensions of the cavity. Fig. 7 shows the Q factor as a function of r_a/r_b for the TM_{110} mode. The resonant frequency of TM_{110} mode is independent of the height of the cavity. To study the effects of the height of the cavity for TM_{110} mode, the minimum and maximum values of the height of the cavity of 0.5λ and infinity, respectively, are used. It can be observed that the Q factor of the TM_{110} mode increases as the height of the cavity increases. The maximum Q factor is obtained when the height of the cavity approaches infinity. The Q factor decreases as r_a/r_b increases. The value of r_a/r_b must first be chosen for a high Q cavity then the values of r_b/λ is selected from the valid region from the desired height of the cavity.

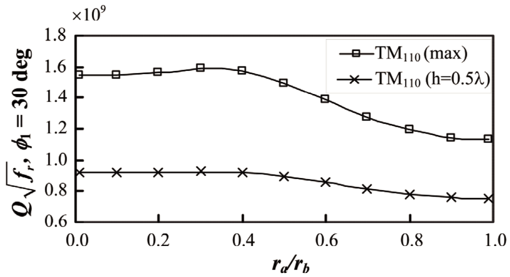

Figure 7. $Q\sqrt{f}$ as a function of r_a/r_b for the TM_{110} mode.

2.4. Resonances of a Concentric Sectoral Cylindrical Cavity

The inner and outer radii of the concentric sectoral cylindrical cavity are obtained from Section 2.3. The suitable parameters for TM_{110} mode are $r_a/r_b = 0.45$, $r_a = 0.507\lambda$ and $r_b = 1.126\lambda$. The cavity yields a high Q and can be easily excited by the coupling slot from the power divider which is a circular waveguide excited by TM_{01} mode. The resonant length, l_R, of the cavity for each mode is shown in Table 1.

Table 1. Resonant length of the cavity for each mode.

Mode	TE_{111}	TE_{011}	TE_{112}	TE_{012}	TE_{113}	TE_{114}	TM_{110}
l_R/λ	0.609	0.887	1.219	1.774	1.828	2.437	Independent with l_R

3. TWO-SLOT ARRAY ANTENNA ON A CONCENTRIC SECTORAL CYLINDRICAL CAVITY

The antenna structure shown in Fig. 8 consists of two parts, the concentric sectoral cylindrical cavity and the circular waveguide shorted at the top end. It is assumed that the TM_{01} dominant mode propagates in the circular waveguide with the inner radius of r_c. The inner and outer radii of the cavity are r_a and r_b, respectively. These parameters are considered from the details in Section 2. The coupling slot S_c is on the circular waveguide and centered at ($r = r_a$, $\phi = 0$, $z = l_{sc}$). The radiating slots, S_1 and S_2 are centered at ($r = r_b$, $\phi = 0$, $z = l_2$) and ($r = r_b$, $\phi = 0$, $z = l_3$), respectively. All slots are circumferentially oriented. The cavity is enclosed by conducting surfaces at the angles of $\phi = -\phi_1$ and $\phi = \phi_1$. The variables l_1 and

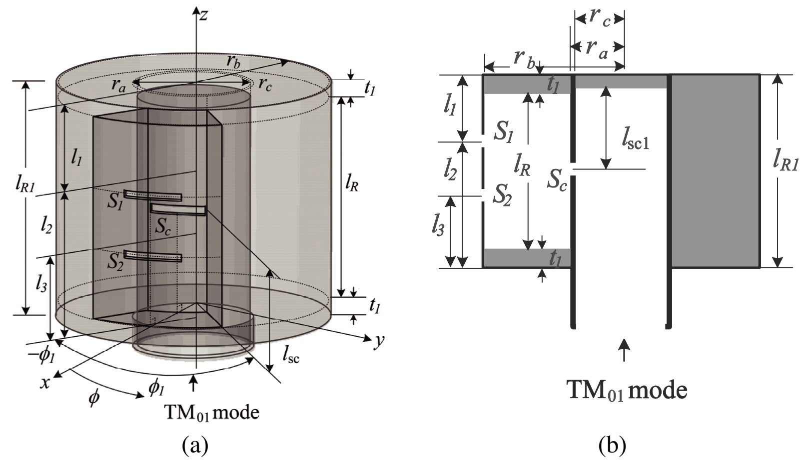

Figure 8. Geometry of a two-slot array antenna on a concentric sectoral cylindrical cavity excited by a coupling slot: (a) in 3 dimensions, (b) in 2 dimensions.

l_3 are the distance from the top of the cavity to the center of the slot S_2 and the distance from the bottom of the cavity to the center of the slot S_1. These distances are fixed at 0.75λ. The spacing between the radiating slots is fixed at 0.5λ, for the maximum directivity and the lengths of the radiating slots are fixed at 0.5λ which is closed to the resonant length given in [22]. The variable l_{sc1}, which is the distance from the shorted end of the circular waveguide to the center of the coupling slot, is fixed at $0.5\lambda_g$, where λ_g refers to the guided wavelength of the TM_{01} mode of the circular waveguide. The thickness of the top and bottom walls of the cavity is represented by t_1. The length of the cavity is l_R. Since l_{R1} is fixed, l_R depends on t_1. The thickness of the walls t is fixed at 2 mm. The other parameters are also listed in Table 2.

4. SIMULATED RESULTS AND DISCUSSION

In this section, the characteristics of the antenna are simulated by using CST Microwave Studio program. The characteristics of the antenna will be investigated as a function of the parameters l_{sc} and l_R.

4.1. Correlations of Magnetic Field Distributions

In this section, the $FIELD_{\text{ant}}$ is simulated by using CST Microwave Studio program. The values of $FIELD_{\text{ant}}$ are volume quantities of the

Table 2. Antenna parameters.

Antenna Parameters	Electrical Size	Physical Size at 5.8 GHz
Inner radius of the cavity (r_a)	0.507λ	26.20 mm
Outer radius of the cavity (r_b)	1.126λ	58.23 mm
Inner radius of the circular waveguide (r_c)	0.469λ	24.20 mm
External length of the cavity (l_{R1})	2.000λ	103.44 mm
Length of the slot S_1 and slot S_2 (L_{S1} and L_{S2})	0.500λ	25.86 mm
Width of the slot S_1 and slot S_2 (W_{S1} and W_{S2})	0.058λ	3.00 mm
Length of the coupling slot (L_{SC})	0.480λ	24.83 mm
Width of the coupling slot (W_{SC})	0.077λ	4.00 mm

cavity. The spacing between each field observation position is fixed in all directions at 2 mm which are sufficiently accurate to determine the correlations of the magnetic field distributions.

The complex values of $FIELD_{\text{ant}}$ is a phasor representation which can be written in terms of a time-harmonic representation as

$$\tilde{H}_{x,y,z}(t) = |H_{x,y,z}| \cos(\omega t + \angle H_{x,y,z}) \tag{28}$$

where $|H_{x,y,z}|$ and $\angle H_{x,y,z}$ are magnitude and phase of $FIELD_{\text{ant}}$ at the observation position $(x,\ y,\ z)$.

The $FIELD_{\text{mode}}$ is the mode distributions of the magnetic field inside the cavity. To find $FIELD_{\text{mode}}$ at a given observation position $(x,\ y,\ z)$, the $(x,\ y,\ z)$ is scaled and transformed to the cylindrical coordinates and used in (7)–(9) and (17)–(19).

The correlation between $FIELD_{\text{ant}}$ from (28) and $FIELD_{\text{mode}}$, $Corr_{\text{mode}}$, for each mode existing in the antenna is given by

$$Corr_{\text{mode}} = \frac{\langle FIELD_{\text{ant}}, FIELD_{\text{mode}} \rangle}{\sqrt{\langle FIELD_{\text{mode}}, FIELD_{\text{mode}} \rangle}} \tag{29}$$

where $\langle\ \rangle$ is an inner product. Fig. 9 shows an example of the correlation of the magnetic field distributions, as a function of ωt when $l_R = 0.9\lambda$ and a center-excited coupling slot is used. It is observed that the maximum values of $Corr_{\text{mode}}$ for each mode existing in the antenna occurred at different ωt. From the result, the $Corr_{\text{mode}}$ can be demonstrated the $FIELD_{\text{mode}}$ of each mode existing in the antenna at each ωt. In addition, the results show that the values of $Corr_{\text{TE111}}$ and $Corr_{\text{TE113}}$ are zero due to the mode cannot be excited.

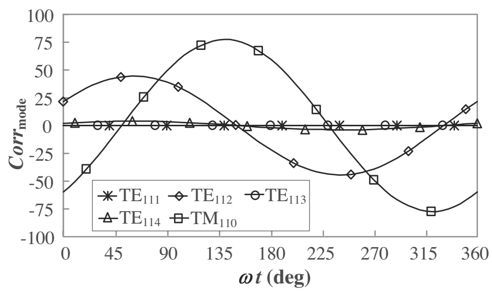

Figure 9. Correlations of the magnetic field distributions as a function ωt with $l_R = 0.9\lambda$.

The total power P_T, is the summation of the power for all significant modes defined as

$$P_T = P_{\text{TM110}} + P_{\text{TE111}} + P_{\text{TE112}} + P_{\text{TE113}} + P_{\text{TE114}} \tag{30}$$

and $P_{\text{mode}}(\%)$ is defined as

$$P_{\text{mode}}(\%) = 100 \cdot P_{\text{mode}}/P_T \tag{31}$$

where $P_{\text{mode}} = |Corr_{\text{mode}}|^2_{\max}$. Fig. 10 shows values of $P_{\text{mode}}(\%)$ as a function of l_R/λ where the values of $P_{\text{mode}}(\%)$ lower than 0.01% is not plotted. When a center-excited coupling slot (or $l_{sc} = l_R/2$) is used, the values of $P_{\text{mode}}(\%)$ of each mode as a function of l_R/λ is shown in Fig. 10(a). It is observed that the maximum and minimum values of $P(\%)_{\text{TM110}}$ occurred at l_R/λ equal to 0.60 and 1.22, respectively. In contrast, l_R/λ of 0.60 and 1.22 yield the minimum and maximum values of $P_{\text{TE112}}(\%)$, respectively. The values of $P_{\text{TE114}}(\%)$ occurred when the values of l_R/λ is greater than 1.6. The values of $P_{\text{TE111}}(\%)$ and $P_{\text{TE113}}(\%)$ are zero due to the mode cannot be excited. When an offset-excited coupling slot (or $l_{sc} = (l_R/2) + 4\,\text{mm}$) is used, a similar trend is observed as shown in Fig. 10(b). However, the values of $P_{\text{mode}}(\%)$ at l_R/λ of 0.6–0.9 and 1.6–1.9 have significant effects from the TE_{111} mode and the TE_{113} mode, respectively.

4.2. Radiation Patterns

Figure 11(a) shows the radiation patterns of the antenna using a center-excited coupling slot. It is obvious that the radiation pattern in xz-plane is independent of l_R. Due to the excitation by a coupling slot

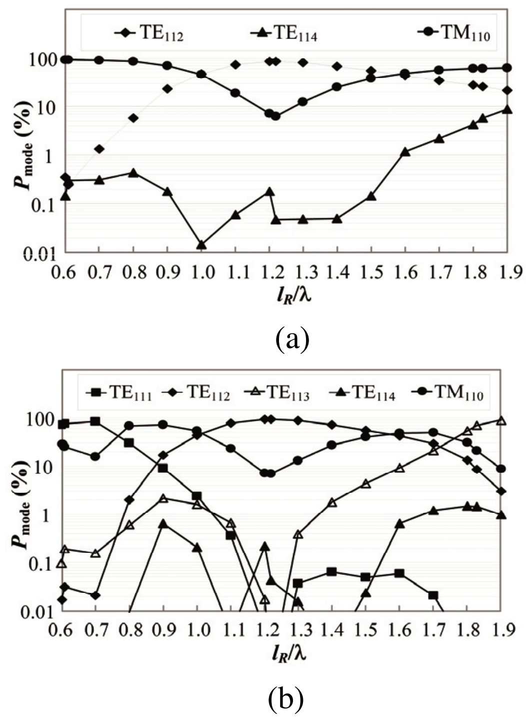

Figure 10. Values of $P_{\text{mode}}(\%)$ as a function of l_R/λ: (a) Center-excited coupling slot, (b) Offset-excited coupling slot.

at the center of l_R, the TE_{111} mode and the TE_{113} mode cannot be generated. Therefore, the magnetic fields at both slots are identical.

The radiation patterns of the antenna using an offset-excited coupling slot are shown in Fig. 11(b). The patterns depend on l_R because the TE_{111} mode and the TE_{113} mode can be excited by the coupling slot. The longer values of l_R/λ has more effects on the radiation pattern than the shorter values of l_R/λ, due to the longer values of l_R/λ can generate more than one mode. The cavity does not contain a pure component mode of the TM_{110} mode. Therefore, the magnetic fields at both slots are not identical. The radiation patterns in xz-plane are tilted downward.

In both cases, the TE_{011} mode and the TE_{012} mode cannot be excited by the coupling slot due to the magnetic field is aligned in the z direction. The TE_{112} mode and the TE_{114} mode can be excited but have no significant effects on the radiation patterns.

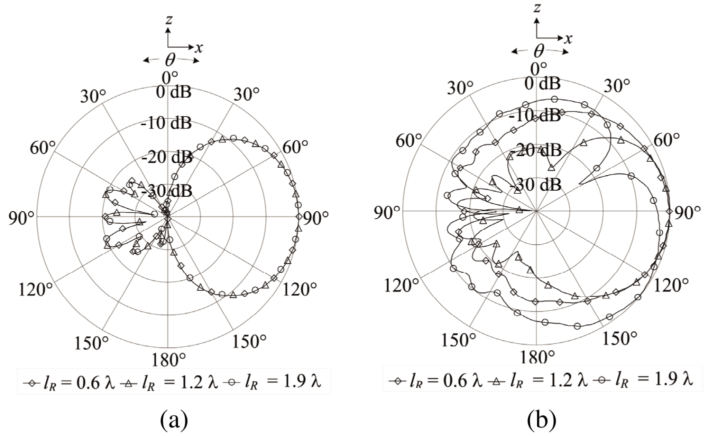

Figure 11. Radiation patterns in xz-plane (a) Center-excited, (b) Offset-excited.

4.3. Directivity and Beam Peak

Figure 12(a) shows the directivity and beam peak in xz-plane as a function of l_R/λ. It is observed that the directivity and the beam peak of the antenna using a center-excited coupling slot are constant at 8.5 dBi and 90 degrees, respectively. When an offset-excited coupling slot is used, the directivity and the beam peak are varied with respect to l_R. The directivity decreases almost monotonically as l_R. The beam peaks are tilted since the TE_{111} mode and the TE_{113} mode are excited. The maximum beam peaks occur at $l_R/\lambda = 0.7$ and $l_R/\lambda = 1.9$, due to the TE_{111} mode and the TE_{113} mode is fully excited, respectively.

4.4. Magnitude of S_{11}

Figure 12(b) shows the magnitude of S_{11} as a function of l_R/λ. When a center-excited coupling slot is used, it is observed that the magnitude of S_{11} increases as l_R/λ increases from 0.60–1.22 and the magnitude of S_{11} decreases as l_R/λ increases from 1.22–1.80. The maximum magnitude of S_{11} occurs at $l_R/\lambda = 1.22$, due to the TE_{112} mode is fully excited at $l_R/\lambda = 1.22$. The magnitude of S_{11} increases as l_R/λ increases from 1.8–1.9, due to the effects of the TE_{114} mode. A similar trend is observed for the antenna using an offset-excited coupling slot. However, the magnitude of S_{11} of the antenna using an offset-excited coupling slot is higher at l_R/λ of 0.6–0.7 and 1.7–1.9 due to the TE_{111} mode and the TE_{113} mode are fully excited, respectively.

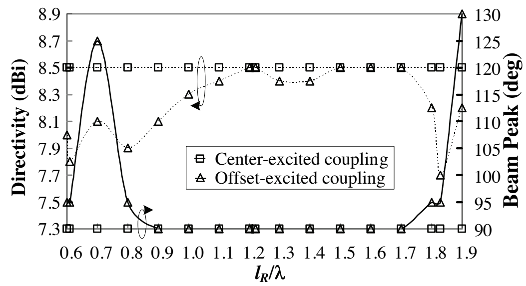

(a)

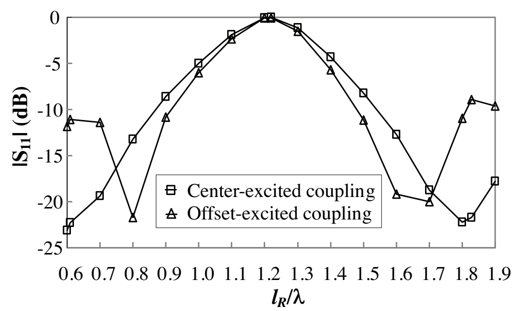

(b)

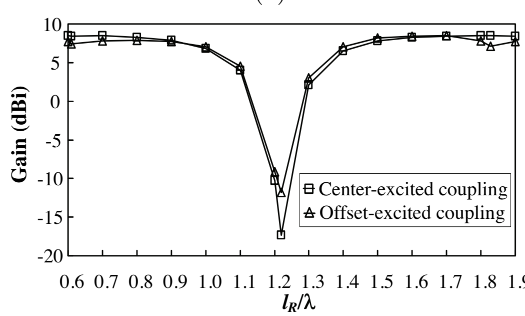

(c)

Figure 12. (a) Directivity and beam peak, (b) Magnitude of S_{11}, (c) Antenna gain.

A pure component mode of the TM_{110} mode is desired for antenna design. When the center-excited coupling slot is used, the TE_{111} mode and the TE_{113} mode cannot be generated. The TE_{112} mode and the TE_{114} mode can be excited but have no significant effects to the radiation patterns. However, the TE_{112} mode and the TE_{114} mode degraded the magnitude of S_{11} and the maximum magnitude of S_{11}

occurred at the mode is fully excited. When the offset-excited coupling slot is used, the TE_{111} mode and the TE_{113} mode can be generated and degrade the radiation patterns due to the magnetic fields at both slots are not identical. In addition, the TE_{111} mode and the TE_{113} mode also degraded the magnitude of S_{11}. Figure 12(c) shows the effects on the antenna gain. The existing of other modes degrades the antenna efficiency and causes the antenna gain to decrease.

Therefore, the center-excited coupling slot must be used for optimum antenna characteristics and l_R must be shorter than the resonant length of the cavity for the TE_{112} mode. This will be used as the design guidelines.

5. MEASUREMENT RESULTS

To verify the simulated results, the prototyped antenna of the two-slot array antenna on a concentric sectoral cylindrical cavity excited by a coupling slot was fabricated at the operating frequency of 5.8 GHz with the parameters in Table 2 and is shown in Fig. 13. The parameter l_R/λ of 0.7 is the suitable design parameter. The monopole on the circular reflector, connected to a SMA connector, is used to excite the TM_{01} mode into the circular waveguide.

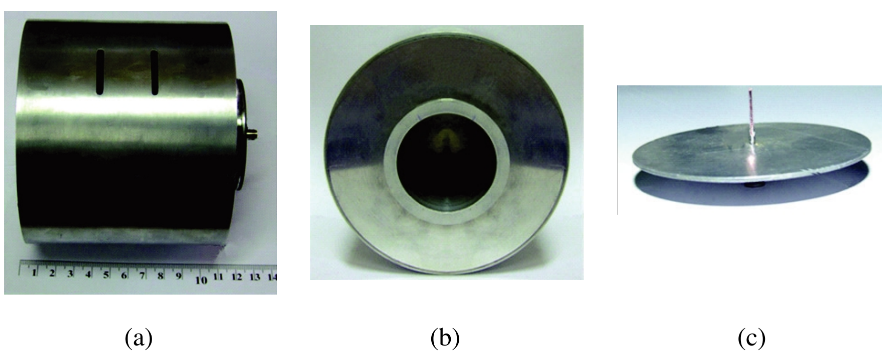

Figure 13. Prototyped antenna: (a) Perspective view, (b) Bottom view, (c) Monopole on the circular reflector.

Figure 14 shows the comparison between the simulated and measured results of the radiation patterns in xy- and xz-planes. The solid and circle lines are denoted the simulated and measured results, respectively. An excellent agreements are obtained in both in xy- and xz-planes. Figure 15 shows the measured magnitude of S_{11}. The return

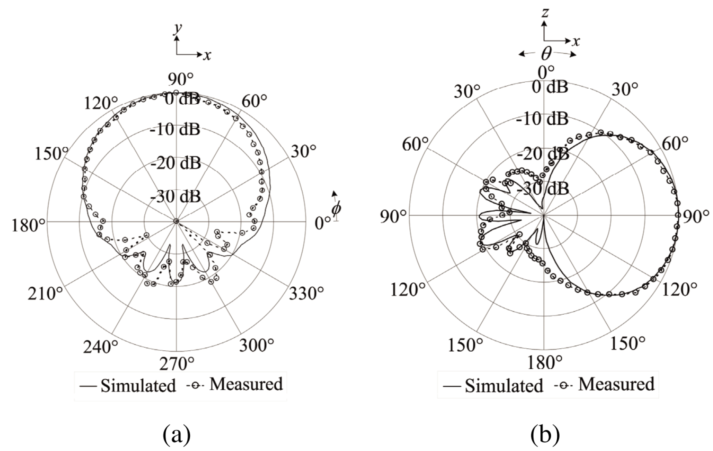

Figure 14. Radiation pattern: (a) xy-plane, (b) xz-plane.

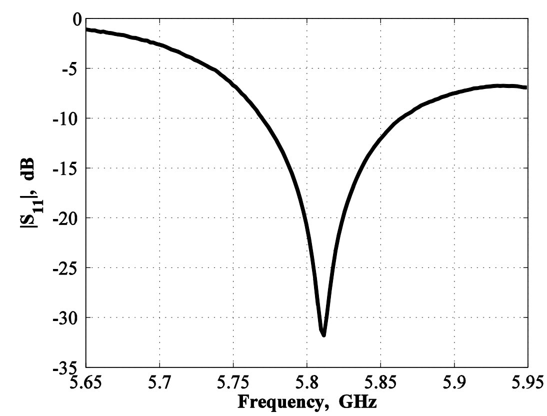

Figure 15. Magnitude of S_{11} of the prototyped antenna.

loss of 20.6 dB is obtained at 5.8 GHz. The measured gain at 5.8 GHz is 7.8 dBi.

6. CONCLUSION

In this paper, a two-slot array antenna on a concentric sectoral cylindrical cavity excited by a coupling slot is investigated. The electromagnetic solutions and Q factors of a concentric sectoral cylindrical cavity are presented. The relations between the outer radius and the ratio of the inner to outer radii are studied. The Q factor is used to determine the optimum dimensions of the cavity. The results show that the appropriate mode for a slot array antenna on a concentric sectoral cylindrical cavity is the TM_{110} mode. The correlations between each mode distribution and the magnetic field distributions inside the cavity are presented. The radiation pattern, magnetic field distribution and magnitude of S_{11} are investigated in the terms of the length of the cavity. The results show that when a center-excited coupling slot is used, the TE_{112} mode and TE_{114} mode degraded the magnitude of S_{11}.To obtain the high efficiency of the antenna, the suitable parameters are the center-excited coupling slot and the length of the cavity must be shorter than the resonant length of the cavity for the TE_{112} mode. The prototyped antenna was fabricated and measured to verify the simulated results. The results provide useful information for the design of a switched-beam slot array antenna on the concentric sectoral cylindrical cavities.

ACKNOWLEDGMENT

This work was supported by the Thailand Research Fund (TRF) under the grant number RTA 5180002.

REFERENCES

1. Liu, H. X., H. Q. Zhai, L. Li, and C. H. Liang, "A progressive numerical method combined with MOM for a fast analysis of large waveguide slot antenna array," *Journal of Electromagnetic Waves and Applications*, Vol. 20, No. 2, 183–192, 2006.
2. Pazoki, R. and J. Rashed-Mohassel, "Bandwidth enhancement of resonant slot array antennas," *Journal of Electromagnetic Waves and Applications*, Vol. 21, No. 9, 1177–1189, 2007.
3. Lim, K. S., V. C. Koo, and T.-S. Lim, "Design, simulation and measurement of a post slot waveguide antenna," *Journal of Electromagnetic Waves and Applications*, Vol. 21, No. 12, 1589–1603, 2007.
4. Mondal, M. and A. Chakrabarty, "Resonant length calculation and radiation pattern synthesis of longitudinal slot antenna in rectangular waveguide," *Progress In Electromagnetics Research Letters*, Vol. 3, 187–195, 2008.
5. Li, L., C.-H. Liang, and C.-H. Chan, "Waveguide end-slot phased array antenna integrated with electromagnetic bandgap

structures," *Journal of Electromagnetic Waves and Applications*, Vol. 21, No. 2, 161–174, 2007.

6. Zhao, X. W., X. J. Dang, Y. Zhang, and C. H. Liang, "MLFMA analysis of waveguide arrays with narrow-wall slots," *Journal of Electromagnetic Waves and Applications*, Vol. 21, No. 8, 1063–1078, 2007.
7. Tiwari, A. K., D. R. Poddar, and B. N. Das, "On the equivalent radius of a radiating slot in impedance calculations," *Progress In Electromagnetics Research*, PIER 74, 47–56, 2007.
8. Hamid, A.-K. and F. R. Cooray, "Radiation characteristics of a spheroidal slot antenna coated with isorefractive materials," *Journal of Electromagnetic Waves and Applications*, Vol. 21, No. 12, 1605–1619, 2007.
9. Shin, D. H. and H. J. Eom, "Radiation from narrow circumferential slots on a conducting circular cylinder," *IEEE Trans. Antennas Propagat.*, Vol. 53, No. 6, 2081–2088, June 2005.
10. Ock, J. S. and H. J. Eom, "Radiation of a hertzian dipole in a short-ended conducting circular cylinder with narrow circumferential slots," *Progress In Electromagnetics Research Letters*, Vol. 2, 11–20, 2008.
11. Hamid, A. K., "Multi-dielectric loaded axially slotted antenna on circular or elliptic cylinder," *Journal of Electromagnetic Waves and Applications*, Vol. 20, No. 9, 1259–1271, 2006.
12. Kim, J. H. and H. J. Eom, "Radiation from multiple annular slots on a circular cylindrical cavity," *Journal of Electromagnetic Waves and Applications*, Vol. 21, No. 1, 47–56, 2007.
13. Wang, J. H. and K. K. Mei, "Theory and analysis of leaky coaxial cables with periodic slots," *IEEE Trans. Antennas Propagat.*, Vol. 49, No. 12, 1723–1732, Dec. 2001.
14. Kim, D. H. and H. J. Eom, "Mode-matching analysis of axially slotted coaxial cable," *IEEE Antennas Wireless Propag. Lett.*, Vol. 4, 169–171, 2005.
15. Ahn, C. H., D. W. Yi, and W. S. Park, "Design of a radiated-mode multislot leaky coaxial cable," *Microw. Opt. Tech. Lett.*, Vol. 45, No. 4, 338–342, May. 2005.
16. Park, J. K., D. H. Shin, J. N. Lee, and H. J. Eom, "A full-wave analysis of a coaxial waveguide slot bridge using the Fourier transform technique," *Journal of Electromagnetic Waves and Applications*, Vol. 20, No. 2, 143–158, 2006.
17. Shin, D. H. and H. J. Eom, "Radiation of a leaky coaxial cable with narrow transverse slots," *IEEE Trans. Antennas Propagat.*,

Vol. 55, No. 1, 107–110, Jan. 2007.

18. Fan, G. X. and J. M. Jin, "Scattering from a cylindrically conformal slotted waveguide array antenna," *IEEE Trans. Antennas. and Propagat.*, Vol. 45, 1150–1159, July 1997.
19. Lin, F. and A. S. Omar, "Segment-sector waveguides," *Proc. 1989 IEEE AP-S Int. Symp.*, 965–968, June 1989.
20. Elsherbeni, A., D. Kajfez, and S. Zeng, "Circular sectoral waveguides," *IEEE Antennas and Propagation Magazine*, Vol. 33, 20–27, Dec. 1991.
21. Lue, S. W., S. C. Li, and S. M. Cao, "Slot antenna in the cuved broad wall of a sectoral waveguide," *Asia-Pacific Microwave Conference 1992*, 401–403, Adelaide, Australia, 1992.
22. Lue, S. W., Y. Zhuang, and S. M. Cao, "The equivalent parameters for the radiating slot on a sectoral waveguide," *IEEE Trans. Antennas Propagat.*, Vol. 42, 1577–1581, Nov. 1994.
23. Wongsan, R., C. Phongcharoenpanich, M. Krairiksh, and J. Takada, "Impedance characteristic analysis of an axial slot antenna on a sectoral cylindrical cavity excited by a probe using Method of Moments," *IEICE Trans. Fundamentals*, Vol. E-86A, 1364–1373, June 2003.
24. Pasri, N., C. Phongcharoenpanich, and M. Krairiksh, "Design of a circumferential slot antenna on a sectoral cylindrical cavity excited by a probe," *Proc. 2004 IEEE AP-S Int. Symp.*, 2337–2340, June 2004.
25. Balanis, C. A., *Advance Engineering Electromagnetics*, John Wiley & Sons, New York, 1989.
26. Miner, G. F., *Lines and Electromagnetic Fields for Engineers*, Oxford University Press, New York, 1996.
27. Harrington, R. F., *Time-Harmonic Electromagnetic Fields*, McGraw-Hill, New York, 1985.